archives
of thermodynamics
Vol. **42**(2021), No. 4, 217–246
DOI: 10.24425/ather.2021.139660

Experimental study of a two-phase ejector for CO_2 transcritical refrigeration system

PHILIPPE HABERSCHILL[a]
EZZEDDINE NEHDI[b]
LAKDAR KAIROUANI[b*]
MOUNA ABOUDA ELAKHDAR[b]

a University of Lyon, CNRS, INSA-Lyon, CETHIL UMR5008, F-69621, Villeurbanne, France

b Research Lab Energetic and Environment, National Engineering School of Tunis, Tunis El Manar University, Tunisia

Abstract The geometry and operating parameters have an important influence on the performance of ejectors. The improvement of the refrigeration cycle performance and the design of the ejectors for the compression energy recovery requires a detailed analysis of the internal ejector working characteristics and geometry. To this aim, an experimental investigation of an ejector refrigeration system is conducted to determine the effect of the most important ejector dimensions on ejector working characteristics and system performance. Different dimensions of ejector components are tested. The influence of the ejector's geometrical parameters on the system performance was analysed. The experiments with respect to the variation of ejector geometry such as the motive nozzle throat diameter, the mixing chamber diameter and the distance between the motive nozzle and diffuser were carried out. There exist optimum design parameters in each test. The experimental results show that the performance (entrainment ratio and a compression ratio of the ejector) increases significantly with the position between the primary nozzle and the mixing chamber. A maximum entrainment ratio of 57.3% and a compression ratio of 1.26 were recorded for the different parameters studied. The results obtained are consistent with experimental results found in the literature.

Keywords: CO_2; Ejector; Transcritical cycle

*Corresponding Author. Email: lakdar_kairouani@yahoo.fr

Nomenclature

A, α	–	angle of primary nozzle divergence, °
α_{dif}	–	diverging angle of the diffuser, °
CR	–	compression ratio (the ratio of static pressures at the diffuser outlet and of secondary flow at the ejector inlet)
COP	–	coefficient of performance
D_d	–	outlet diameter of the diffuser, mm
d_s	–	outlet diameter of the primary nozzle, mm
d^*	–	throat diameter of the primary nozzle, mm
d_m	–	diameter of the mixing chamber, mm
L_m	–	length of the mixing chamber, mm
P	–	pressure, MPa
q_{m_p}	–	primary mass flow rate, g/s
q_{m_s}	–	secondary mass flow rate, g/s
T	–	temperature, °C
T_0	–	evaporation temperature, °C
U	–	entrainment ratio, $= q_{m\_p}/q_{m\_p}$
X	–	distance between the motive nozzle and mixing chamber, mm
X_{opt}	–	optimum distance between the motive nozzle and mixing chamber, mm
X^*_{opt}	–	dimensionless optimum distance, $= X_{opt}/d_m$

Acronyms

EERC	–	ejector expansion refrigeration cycle
GC	–	gas cooler
P	–	primary
PN	–	primary nozzle
S	–	secondary
V	–	valve
VLS	–	vapor-liquid separator

1 Introduction

The reduced refrigeration production and the low coefficient of performance (COP) at high outdoor temperatures represent a major disadvantage of transcritical CO_2 (carbon dioxide) systems [1]. The high working pressures and in particular the large pressure differences between the evaporator and the cooler make R744 an ideal fluid for the recovery of the expansion work because the differences between isenthalpic expansion and isentropic expansion became more obvious.

Liu *et al.* [2] used the Kornhauser modelling approach and calculated an improvement in theoretical COP between 6% and 14%, for a two-phase ejector transcritical CO_2 system. Jeong *et al.* [3] studied by numerical simulation the characteristics of a two-phase ejector and the performance of the cycle operating with an ejector. They assumed an ejector efficiency of

0.9 and found that the COP of the CO_2 cycle with the ejector was 22% higher than that of the cycle without the ejector.

Deng *et al.* [4] carried out a theoretical analysis of a refrigeration machine with expansion by a transcritical CO_2 ejector. They assumed an efficiency of 0.7 of the driving nozzle of the ejector and found that the maximum COP is 22% higher than the COP of a conventional vapour compression cycle and 18.6% higher as compared to the system with an internal heat exchanger. They found that the cooling capacity of the ejector cycle is 11.5% higher than that of the conventional cycle. In addition, the performance of the ejector cycle was found to be very sensitive to operating conditions.

Li and Groll in 2005 assume a diffuser efficiency of 0.8 in the model of a CO_2 refrigeration machine with an ejector [5]. They found that the COP of the ejector CO_2 transcritical cycle can be improved by more than 16% compared to the conventional transcritical CO_2 cycle for the operating conditions of an air conditioning system. Ksayer and Clodic in 2006 assume the efficiency of the driving nozzle equal to 0.85 and a diffuser efficiency of 0.75 in an ejector model with a constant pressure mixing chamber [6]. They found that the COP of the transcritical CO_2 ejector cycle can be improved by over 15% compared to the conventional transcritical cycle for typical air conditioning operating conditions.

The modelling of ejectors is still a very diverse and evolving area of research. The models are classified into three families: computational fluid dynamics (CFD), thermodynamics and empirical or semi-empirical [8]. Recent research on numerical models is very active and continues to improve our understanding of specific local effects on the ejector [9–17]. Although these models offer advantages in terms of the accuracy of the results, they are very complex. CFD modelling can accurately predict the ejector performance for critical mode and subcritical mode operation, but models can generate entrainment ratio errors of 40–50% [18]. 1D methods are simpler and less expensive than CFD techniques [19]. They are, however, difficult to implement compared to thermodynamic methods because this approach remains linked to the resolution of partial differential equations. Thermodynamic methods are the most widely used for two-phase ejector models and their main advantage is their ability to generate results very quickly.

Kornhauser developed one of the first thermodynamic models for two-phase ejectors [20]. The approach was based on the HEM (homogenous equilibrium model) and the constant pressure mixing hypothesis, commonly used in ejectors. Isentropic efficiencies are used to take into account the pressure drops in the primary nozzle and in the diffuser. The constant

pressure is imposed during the mixing process, where no friction and losses are considered during mixing. Kornhauser's model has been used by many researchers [5, 21] and remains popular due to its simplicity. However, this approach has a number of weaknesses, for example, selecting the isentropic efficiency of a thermodynamic model can be difficult, especially for a two-phase flow [22].

The experimental results of Elbel and Hrnjak revealed in 2008 that the ejector simultaneously improves cooling production and COP by up to 7% and 8%, respectively, in the CO_2 system [1]. Liu *et al.* [22] designed an adjustable ejector for CO_2 air conditioning. The effect of the ejector geometry (throat diameter of the driving nozzle and distance between motive nozzle and mixing chamber (X) on the entrainment ratio, the compression ratio, the cooling capacity and the compressor consumption power have been studied experimentally. They concluded that a driving nozzle throat diameter (d^*) of 1.8 mm and a distance X of 12 mm achieve the highest COP. As some experimental tests suggest, many authors have set these efficiencies lower than they typically are in single-phase ejectors. For Lawrence and Elbel, for example, the efficiency of the primary nozzle, the secondary nozzle and the diffuser are equal to 0.8, 0.8 and 0.75, respectively, [23].

Liu *et al.* [22] in 2012 performed a numerical analysis of the geometry of CO_2 ejectors, for a 1D model of the ejector to determine its dimensions. The COP of the transcritical CO_2 cycle with an ejector is very sensitive to the efficiency of the ejector [24]. However, the knowledge of the efficiency of the ejector is very limited in the literature. Sarkar assumed a nozzle efficiency of 0.8 and that of the diffuser of 0.75 in the modelling and simulation of the cycles of ejector CO_2 transcritical heat pumps [25].

Varga *et al.* [26] in 2009 studied numerically (CFD) the influence of the geometry of the selected parameters, namely, the area ratio between the driving nozzle and the mixing chamber, the position of the outlet plane of the nozzle and the length of the mixing chamber, on the performance of a steam ejector. The results indicate the existence of optimal values ??for these three parameters.

Elbel and Hrnjak, in 2004, used Kornhauser's approach to study numerically the effect of adding an internal heat exchanger on the performance of a transcritical R744 system with an ejector [21]. They have shown that the highest COPs can be obtained with an ejector and an internal heat exchanger. In 2008 they [1] experimentally studied a transcritical CO_2 system using an ejector with different dimensions of the driving nozzle and the diffuser. They found that the ejector efficiency is affected by the section at the

driving nozzle throat and the angle of the diffuser. The highest efficiencies are obtained when the diffuser angle is 5°. Elbel (in 2011) presented more results on how the performance of the CO_2 ejector is affected by variations in geometry, namely the diverging angle of the diffuser and the length of the mixing chamber [27]. The best ejector performance recorded was obtained for the diverging angle of the diffuser, $\alpha_{\text{dif}} = 5°$.

Lee *et al.* [28] presented experimental results obtained using a transcritical CO_2 refrigeration system with an ejector expansion and internal heat exchanger. They showed that the refrigeration COP is about 15% higher than that of the conventional system and the COP reaches the maximum when the entrainment rate is 0.9.

Banasiak and Hafner presented a study of the influence of the geometry of the ejector (the diameter of the mixing chamber, its length and the angle of the diffuser) on its efficiency [29]. The efficiency of the ejector reveals a maximum for high pressure. The results regarding the length and diameter of the mixing chamber are similar to the data published by Nakagawa *et al.* [30, 31]. The data shows an optimum length and an optimum diameter of the mixing chamber. The variation of the diffuser angle shows maximum ejector efficiency with a diffuser angle of 5°. The data agree with the results of Elbel and Hrnjak [1]. The maximum ejector efficiency is 34%.

Several parameters determine the performance of the CO_2 refrigeration installation. These parameters are the entrainment ratio, the temperature at the outlet of the gas cooler, the evaporation temperature and the geometry of the ejector (diameter of the mixing chamber, length of the mixing chamber, throat diameter of the primary nozzle, divergent angle of the primary nozzle, the distance between the primary nozzle and the inlet of the constant section of the mixing chamber). To clarify the influence of these parameters on the performance of the installation, an experimental study was carried out with the aim of:

- determining the parameters that really affect these performances,
- studying the evolution of these performances according to these quantities.

The experimental tests relate to:

- the distance between the primary nozzle and the inlet of the constant section of the mixing chamber for different angles of the primary nozzle divergent,

- the throat diameter and the diverging angle of the primary nozzle,
- the diameter and length of the mixing chamber,
- thermodynamic parameters (evaporation temperature, temperature at the inlet of the primary nozzle for various geometries).

The objective of this work is to make an experimental contribution to the study of transcritical CO_2 refrigeration systems equipped with a two-phase ejector.

Significant efforts have been invested in the design of a two-phase ejector with various geometries to evaluate the main characteristics, namely, the entrainment ratio and the compression ratio.

2 System description

A two-phase ejector can be used to improve the performance of a refrigeration system by reducing the compressor ratio. The CO_2 transcritical cycle and the pressure-enthalpy (P-h) diagram are shown in Fig. 1. It should be noted that the mass flow rate through the gas cooler is not the same as the flow rate of the evaporator. Theoretically, the expansion is assumed to be an isenthalpic transformation. The use of an ejector as an expansion device will change the process from isenthalpic to isentropic. The isentropic process is represented by the transformation between points 4 and 5.

Figure 1 shows the representation of the ejector expansion refrigeration cycle (EERC). In the ejector expansion refrigeration cycle, there are two flows: the primary flow and the secondary flow. While the primary stream is circulated through the compressor, the gas cooler, the ejector, and the separator (points 1, 2, 3, 4, and 5, 7, 8, 9, and 1), the secondary fluid flows through the expansion valve, in the evaporator, the ejector and the separator (points 10, 11, 12, 6, 7, and 8). The mixture of primary and secondary flows carried out at a constant cross-section passes through the diffuser (points 7 and 8). In the ideal cycle, the saturated vapour that comes from the vapour-liquid separator enters the compressor and is compressed isentropically at high pressure and temperature. The heat is rejected in the gas cooler. In the primary nozzle, the supercritical primary fluid is expanded isentropically at the pressure of the mixture. During the expansion process, the primary fluid gains kinetic energy. As shown in Fig. 1, the pressure at point 1 is greater than that at suction in the standard cycle (point 12). The necessary compressor work will be less than that of the standard cycle.

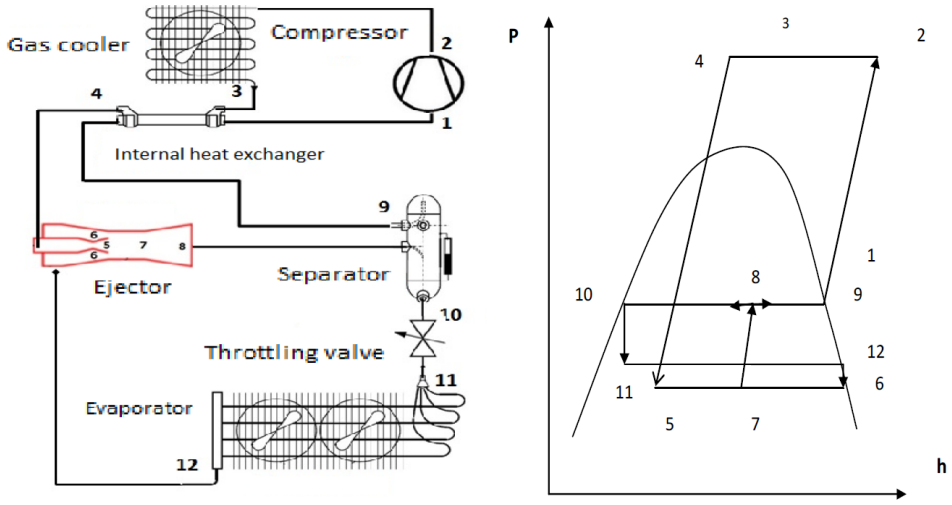

Figure 1: Transcritical CO_2 refrigeration cycle: the ejector expansion refrigeration cycle and the pressure-enthalpy diagram.

3 Experimental apparatus

The experimental study is carried out on the test bench of an air/water refrigerating machine using CO_2 as a refrigerant installed at the Centre for Energy and Thermal Sciences of Lyon (CETHIL) at the National Institute for Applied Sciences (INSA Lyon). This installation is composed of three circuits independent of each other. The first is the CO_2 circuit. The second is an auxiliary water circuit whose temperature and flow rate are controlled to simulate the variation of the parameters of the hot source. The third is an air circuit regulated in temperature and hygrometry to simulate the variations of the climatic conditions. The diagram of the installation is given in Fig. 2. Several measurements of temperatures, pressures and flow rates are implemented in the fluid circuit of the refrigeration machine and in the two auxiliary circuits in order to analyse the operation of the installation. The signals provided by the measuring instruments are collected in an electronic card. A Keithley multimeter is used to convert and record these different signals. The Keithley is computer-controlled using an ExceLINX driver program developed under Microsoft Excel. This program makes it possible to acquire measurement data on the Keithley and to follow in real time the evolution of various parameters of the installation. In what follows, we will focus only on the CO_2 circuit and the details of the ejector.

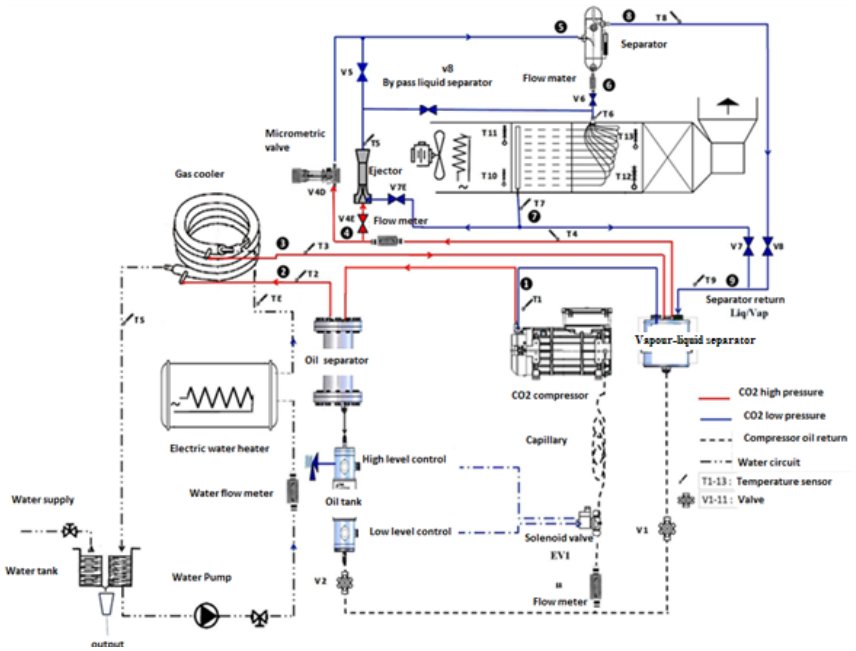

Figure 2: Experimental apparatus.

3.1 CO_2 circuit

The system basically contains the following components:

- a Bock RKX26/31-4 brand 6-cylinder semi-hermetic radial piston compressor powered by a Danfoss variable speed drive to obtain speeds from 0 to 1450 rpm,
- a coaxial water and a high-pressure exchanger for cooling the gas,
- a vapour-liquid separator (VLS) with a heat exchanger,
- a micrometric expansion valve,
- an air evaporator,
- an oil separator with an oil return control device,
- a set of valves VB, V4D, V4E, V5, V6, V7E, V7 and V8, which make it possible to switch from a valve expansion to an operation with the ejector as an expansion device in order to compare the performance of the machine in both cases and for the same operating conditions.

However, the valve VB will serve as a bypass of the vapour-liquid separator,

- pipes, hoses and other devices, in which the refrigerant CO_2 evolves, to complete a refrigerating cycle.

The details of the measurement apparatus as well as the measurement accuracy are indicated in Table 1.

Table 1: Measurement range and accuracy of each instrument.

Instrument	Range	Accuracy	Location
Measurement on the CO_2 circuit			
09 Type K thermocouples	–30–170°C	±0.5 °C	Centre of the CO_2 tubes
Differential pressure transmitters	0–10	0.2%	Gas cooler inlet/outlet
Absolute pressure transmitter	0–100 bar	0.25%	Compressor suction
Absolute pressure transmitter	50–150 bar	0.5%	Compressor discharge
Absolute pressure transmitter	0–160 bar	0.5%	Ejector inlet
Differential pressure transmitter	0–10 bar	0.2%	Gas cooler inlet/outlet
Differential pressure transmitter	0–10 bar	0.2%	Suction line
Differential pressure transmitter	0–10 bar	0.2%	Liquid line
Differential pressure transmitter	0–3.50 bar	0.25%	Diffuser and evaporator outlet
02 Coriolis flowmeter	0–300 g/s	0.5%	Measurement of primary flow and secondary flow
Measurement on the air circuit			
04 Type K thermocouples	20–50°C	±0.5 K	Ventilation duct
Measurement on the water circuit			
2 Pt100 probes		±0.25 K	Water temperature measurement
01 Electro-magnetic flowmeter	0–2000 kg/h	0.2%	Water flow measurement

The carbon dioxide in the form of subcritical vapour (Fig. 2) enters the compressor at the pressure $P1$ in the state (1), where it is adiabatically compressed to the pressure $P2$. In order to prevent the lubricating oil from being drawn into the refrigerant circuit, an oil separator is installed at the discharge of the compressor. To know the flow, the separated oil is sent back to a buffer tank. Two sensors and a solenoid valve make it possible to control the level in this tank and ensure the return of the oil to the crankcase of the compressor after measuring its flow. The CO_2 in the supercritical state at the oil separator outlet is cooled in the gas cooler to the temperature corresponding to the state (3). Then, it crosses the coil of

the vapour-liquid separator. The latter placed on the suction pipe near the compressor is intended to prevent the accidental aspiration of liquid fluid by the compressor, which avoids any mechanical incident. The coil heat exchanger, acting as an internal heat exchanger, improves the evaporation of the refrigerant aspirated by passing the fluid from the gas cooler through the bottom of vapor-liquid separator. This method has the advantage of increasing the subcooling of the fluid at the inlet of the expansion member and highly improving the performance of the refrigeration plant by slightly increasing the cooling capacity. To accurately judge the efficiency of the oil separator, vapour-liquid separator was designed without the oil-return hole usually encountered on this component. Despite the presence of the separator, the oil entrained in the circuit will be retained at the bottom of the VLS. The return of this oil is done manually every hour. The micro-flowmeter measures the amount recovered.

In operation without an ejector, the valves V4E, V5, V7E and VB are closed. The fluid from the coil of the vapour-liquid separator passes through a Coriolis flow meter placed at the inlet of the V4D manual micrometer expansion valve. At the outlet of the latter, the low pressure fluid is injected into the liquid/vapour separator. The act of injecting CO_2 into the latter makes it possible to obtain two phases: the liquid recovered at the bottom of the separator enters the evaporator by passing through the valve V6 and the second flow meter; the vapour at the outlet of the evaporator passes through the valve V7 and mixes with the steam at the temperature T8 withdrawn from the vapour-liquid separator by flowing through the control valve (V8). Finally, the mixture of the two flows through the VLS before being sucked by the compressor.

In operation with an ejector, the valves V4E, V5 and V7E are open, the valve (VD) is closed, and the control valve (V8) is fully open. The supercritical CO_2 at the output of the Coriolis flow meter enters the primary nozzle of the ejector (Fig. 2) with the stagnant characteristics $T4$ and $P4$ combined with those of the state (4), then undergoes expansion in this nozzle. At the outlet, the primary fluid, at supersonic velocity, drives the secondary fluid (S) coming from the evaporator with the temperature and the pressure of the stagnation state ($T7$, $P7$) assumed to be merged with those of the state (7). The primary (P) and secondary (S) flows then mix in the mixing chamber. A first increase in pressure due to the formation of a right shock wave occurs in the cylindrical portion of the mixing chamber followed by a second increase due to the compression in the diffuser. At the outlet of the ejector, the mixture is in the two-phase state (5). The saturat-

ing vapour in the state (9) is sucked by the compressor through the VLS while the liquid saturated at the bottom of the liquid/vapour separator in the state (6) passes through the flow meter and the valve V6 before entering the evaporator to produce the expected cooling effect.

3.2 Ejector

The design of the ejector prototype shown in Fig. 3 required the assembly of five essential elements:

- primary nozzle,
- mixing chamber and diffuser,
- adjustment shim for changing the position of the primary nozzle relative to the mixing chamber,
- support for the primary nozzle (1 piece),
- support of the suction chamber (1 piece).

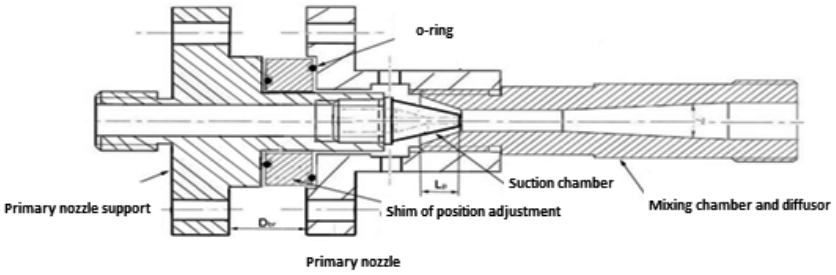

Figure 3: Ejector design.

The geometric parameters of the ejector, namely the angles of the convergent and the divergent of the primary nozzle, the length of the mixing chamber and the diffuser angle are indicated in the literature [5, 17, 21, 25, 26, 28, 29].

The primary nozzle (shown in Fig. 4) is placed on a support. The secondary nozzle formed by the suction chamber, the mixing chamber and the diffuser (Fig. 3) is separated from the support of the primary nozzle by wedges having different thicknesses to experimentally determine the influence of the primary nozzle position relative to the mixing chamber inlet.

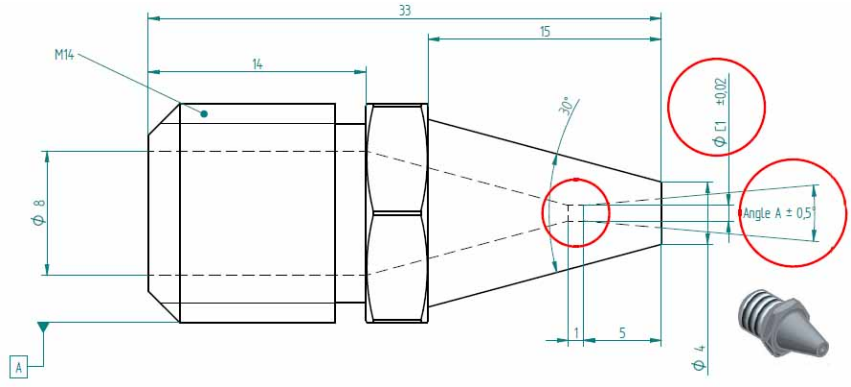

Figure 4: Primary nozzle description.

3.2.1 Primary nozzle

The experimental nozzles have been designed as a convergent-divergent conical channel pierced in the nozzle section. The main construction parameters are as follows (Fig. 4):

- diameters: 8 mm for the inlet section, 0.7 mm to 1.2 mm for the throat;
- cone angles: 30° for the converging section and 2° at 10° for the diverging section;
- roughness of the surface: approximately 10^{-6} m for both sections.

The details of construction of the different nozzles are indicated in Table 2 which specifies the dimensions of the five primary nozzles tested.

Table 2: Characteristics of primary nozzles.

Label	PN1	PN2	PN3	PN4	PN5
$\phi C1 = d^*$ (mm)	1.2	1	0.9	0.9	0.9
Angle A, (°)	2	2	2	5	7

3.2.2 Mixing chamber and diffuser

The mixing chamber and the diffuser make a unique piece. This element was manufactured as a straight tube with a conical shaped inlet, which in combination with the head of the nozzle section forms the suction chamber.

The converging angle for the inlet cone was set at 48° to provide the largest possible passing section, while the internal diameter values (d_m) for the produced pieces ranged from 2.7 mm to 5 mm. Table 3 gives the different dimensions for the 7 mixing chambers manufactured.

Table 3: Different dimensions for the 7 mixing chambers manufactured with the diffusers with angle $\alpha_{\text{dif}} = 7°$.

Label	d_m (mm)	L_m (mm)	L_d (mm)
M1	5	25	57
M2	4	25	32.7
M3	3	25	41
M4	3	12.5	41
M5	3	40	41
M6	2.7	12.5	41
M7	2.7	40	41

The converging input portion was used to have better constant pressure mixing. All the diffusers included an angle $\alpha_{\text{dif}} = 7°$, recommended by Liu and Groll [32–34], in order to find a balance between the effects of deterioration of the performance caused by the separation of the boundary layer (too large angles) and the excessive pressure drop by friction (too small angles).

The diffuser is formed of a diverging conical channel (Fig. 5). The total length of the passage is dependent on the inlet and outlet diameters, and the angle of divergence. The diffuser outlet diameter (D_d) was nominally manufactured to be 8 mm.

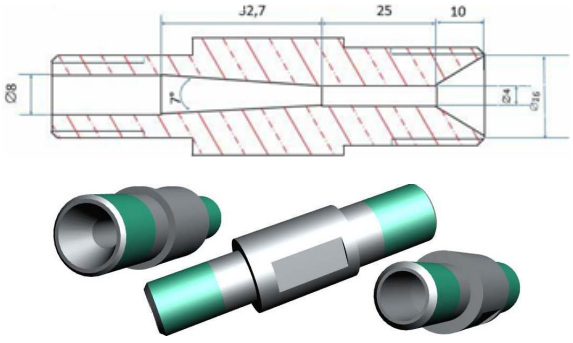

Figure 5: Mixing chamber and diffuser.

3.2.3 Suction chamber

The suction chamber is an annular region surrounding the primary nozzle. It is the space between the outlet section of the primary nozzle and the conical-shaped inlet of the tube forming the mixing chamber and the diffuser. The geometry of the suction chamber is shown in Figs. 3–6. An end flange is assembled with the support of the primary nozzle after centring and positioning of the latter, tapping to another end for receiving the mixing chamber and the diffuser. Two holes on the side aspire to give the secondary fluid.

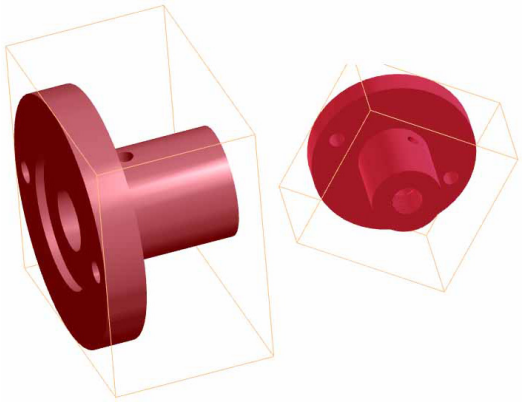

Figure 6: Suction chamber.

3.2.4 Adjustment wedges

Spacer rings or adjustment wedges, Fig. 7, make it possible to vary the position of the driving nozzle tip with respect to the beginning of the mixing section. The reference point for nozzle exit ($X = 0$ mm) is defined as the

Figure 7: Adjustment wedges.

position where the nozzle exit touches the converging part of the mixing chamber wall and thus entirely blocks the passage for the secondary flow.

4 Experimental results: Influence of the position of the primary nozzle

Several authors have studied the influence of the distance between the motive nozzle and mixing chamber (X) on the performance of the ejector and have indicated the existence of an optimum position [7, 35–39].

The ejector tests for different geometries are performed for different pressure levels of the primary flow, ranging from 60 bar to 110 bar. The compressor discharge pressure is adjusted by adjusting the cooling water flow of the gas cooler and its temperature. The compressor speed is kept constant in these experiments. In other tests, the effect of the rotational speed of the compressor is analysed to find the optimum speed giving the best entrainment ratio and the best compression ratio. Control of the power absorbed by the compressor is carried out. A power exceeding 4.7 kW is a compressor overload and can cause a major system failure.

In order to determine the best position of the primary nozzle, the ejector was removed and a wedge was inserted between the flanges to achieve the zero position of the primary nozzle relative to the mixing chamber. Wedges of increasing thickness allow the primary nozzle to be retracted to study the influence of this position on the evolution of the secondary flow rate as a function of the outlet pressure of the gas cooler.

The purpose of this chapter is to highlight the influence of the position of the primary nozzle on the ejector's performance for different diverging angles of the primary nozzle. Four different angles of the divergence – 2°, 5°, 7° and 10° are analysed for different diameters of the throat. For this analysis, the angle of the divergence is 2°.

Three primary nozzles are tested, the geometries of which are listed in Table 4. Initially, these tests are carried out for different CO_2 temperatures

Table 4: Main characteristics of primary nozzles.

Label	d^* (mm)	α (°)	d_s (mm)	$(d_s/d^*)^2$
PN1	1.2	2°	1.54	2.37
PN2	0.9	2°	1.24	1.89
PN3	1.0	2°	1.34	1.79

at the outlet of the gas cooler and the evaporator. These temperatures are kept constant during the experiment. The optimum position of the primary nozzle is that corresponding to a maximum entrainment ratio.

The geometry of the ejector was analysed for different pressure levels of the primary flow, from 70 to 110 bar. The inlet temperature of the motive flow is kept constant at ±0.25 K of the desired temperature. As recommended by the compressor manufacturer, by adding or discharging a quantity of CO_2 from the installation, the parameters on the suction side have been kept constant for the desired pressures at ±0.15 bar and a maximum superheat of 291 K at the compressor suction.

4.1 Case of the primary nozzle PN1

Table 5 illustrates the effect of the distance between the motive nozzle and mixing chamber position on the entrainment ratio (U) of the system. The workout rate of the system is significantly dependent on X, and an optimum position (X_{opt}) exists. For a variable CO_2 temperature of 30°C to 66°C at the outlet of the gas cooler (T_{GC}) and a variable evaporation temperature (T_o) of −8° C to 3° C, the maximum entrainment ratio of the system can reach 0.53 as shown in Table 5. From position $X = 9$ mm, the position X is changed by 2 mm to 4 mm. The variation in the CO_2 pressure at the inlet of the primary nozzle is obtained by adjusting the water flow rate of the gas cooler, which causes a variation in the temperature at the inlet of the ejector. The test is stopped once the temperature of the water leaving the cooler reaches 100°C. The speed of the compressor is kept constant at 900 rpm. It can be seen from Table 5 that the optimum X is between 9 mm and 13 mm. This is entirely in agreement with the study of Eames *et al* [39] who found that the optimum X is in the interval 0 to 15 mm.

For a primary fluid pressure of 75 bar and when X varies from 9 mm to 11 mm, the entrainment ratio increases from 0.21 to 0.35. Then, the entrain-

Table 5: Effect of the distance between the motive nozzle and mixing chamber (X) on the entrainment ratio (U) for different pressures at the inlet of the primary nozzle with the 3 mm diameter mixing chamber (PN1, $d_m = 3$ mm, $L_m = 25$ mm).

	75 bar	80 bar	85 bar	90 bar	92 bar
X (mm)	U	U	U	U	U
9	0.219	0.284	0.368	0.391	0.418
11	0.351	0.400	0.454	0.511	0.535
13	0.323	0.388	0.421	0.492	0.519

ment ratio decreases to 0.32 as X goes from 11 mm to 13 mm. Likewise, for a primary fluid pressure of 92 bar as X increases from 9 mm to 11 mm, the entrainment ratio increases from 0.41 to 0.53. Then, the entrainment ratio decreases to 0.51 as X increases from 11 mm to 13 mm.

The influence of the position of the primary nozzle on the compression ratio (CR) of the ejector is presented in Table 6, showing that the distance $X = 11$ mm gives the maximum compression ratio. For this distance considered to be optimum, the difference between the compression ratio of the ejector at this position with that obtained for other positions is relatively large. It appears, in view of the experiments at constant temperature, that the best obtained compression ratio is 1.26 for a pressure at the inlet of the primary nozzle of 92.7 bar. It is found from Tables 5 and 6 that the increasing driving pressure decreases the entrainment ratio and increases the compression ratio.

Table 6: Effect of the distance between the motive nozzle and mixing chamber (X) on the compression ratio (CR) for different pressures at the inlet of the primary nozzle with the 3 mm diameter mixing chamber ($d_m = 3$ mm, $L_m = 25$ mm; $T_0 = -5^\circ$C; $T_{GC} = 48^\circ$C).

X (mm)	P (bar)	CR	P (bar)	CR	P (bar)	CR	P (bar)	CR	P(bar)	CR
9	84.930	1.170	87.900	1.195	88.972	1.196	90.495	1.195	92.442	1.195
11	86.124	1.239	88.715	1.244	90.312	1.254	92.691	1.263	–	–
13	85.134	1.187	86.980	1.192	88.885	1.195	90.468	1.198	92.018	1.202

Figure 8 shows that the distance X has no effect on the primary flow, which presents a linear variation as a function of the pressure at the inlet of the

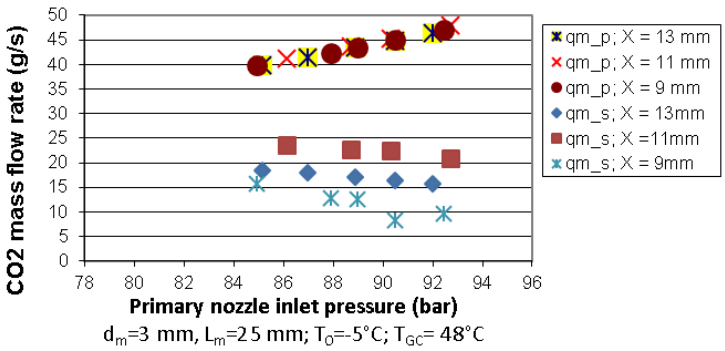

Figure 8: Effect of X on the primary and secondary flow rates for different pressures at the inlet of the primary nozzle with the 3 mm diameter mixing chamber.

primary nozzle. On the other hand, the secondary flow rate is strongly influenced by the outlet position of the primary nozzle. When X increases from 9 mm to 11 mm, the secondary flow varies from 15.82 g/s for a primary fluid pressure of 84.92 bar to 23.67 g/s for a slightly higher pressure of 86.12 bar. When X increases from 11 mm to 13 mm, the secondary flow decreases to 18.42 g/s for a pressure of 85.13 bar.

4.2 Case of the primary nozzle PN2

In order to determine the optimum position for the nozzles having a diverging angle of 2°, the experimental study is continued with the PN2 nozzle having a throat diameter of 1 mm. For a constant CO_2 temperature at the outlet of the gas cooler equal to 45°C and evaporation temperatures of −10°C and −7.5°C, the maximum entrainment rate of the system can reach 0.425. It can be seen from Table 7 that, for a primary fluid pressure of 91 bar and when X increases from 9 mm to 13 mm, the entrainment ratio increases from 0.304 to 0.358. The position $X = 11$ mm gives an entrainment ratio of 0.331 for a pressure of 90 bar. The position $X = 13$ mm is an optimum position in this case, mainly due to the difference in evaporation temperatures. This will be observed when studying the influence of the evaporation temperature. The curve for a temperature of −10°C is shifted to the left and down compared to that obtained for a temperature of −7.5°C. The difference between the entrainment ratio for position $X = 9$ mm and 13 mm is significant.

Table 7: Effect of the distance between the motive nozzle and mixing chamber (X) on the entrainment ratio (U) for different pressures at the inlet of the primary nozzle with the 3 mm diameter mixing chamber ($d_m = 3$ mm, $L_m = 25$ mm; $T_0 = -10$°C and −7.5°C for $X = 13$ mm; $T_{GC} = 45$°C).

X (mm)	P (bar)	U	P (bar)	U	P (bar)	U	P (bar)	U	$^*P$ (bar)	U
9	85.418	0.425	88.576	0.368	90.959	0.305	93.099	0.220	–	–
11	87.961	0.394	90.275	0.331	92.583	0.279	94.222	0.210	95.841	0.194
13	91.055	0.359	92.961	0.319	94.168	0.294	95.396	0.273	96.328	0.196

Figure 9 shows that the distance X has no effect on the primary flow, which presents a linear variation as a function of pressure at the inlet of the primary nozzle. On the other hand, the secondary flow, Fig. 10, is strongly influenced by the exit position of the primary nozzle. When X goes

from 9 mm to 11mm, the corresponding secondary flow presented in Fig. 10 changes from 11.5 g/s for a pressure of 88.5 bar to 12.5 g/s for a pressure of about 88 bar. When X increases from 11 mm to 13 mm, the secondary flow increases and changes from 9.94 g/s to 11.36 g/s for a pressure of 92.5 bar.

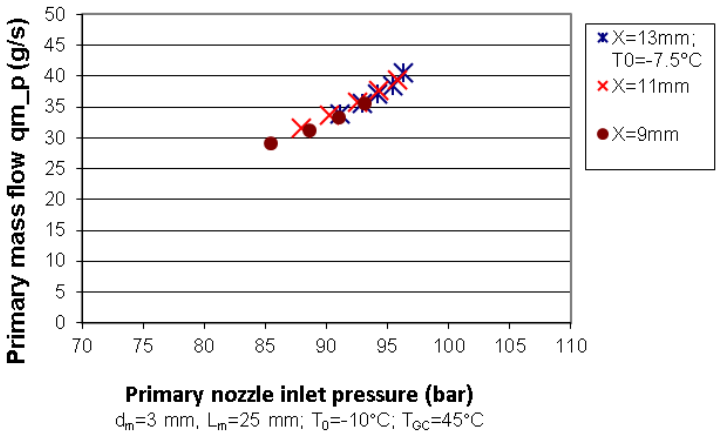

Figure 9: Effect of the distance X on the primary mass flow for different pressures at the inlet of the primary nozzle with the 3 mm diameter mixing chamber.

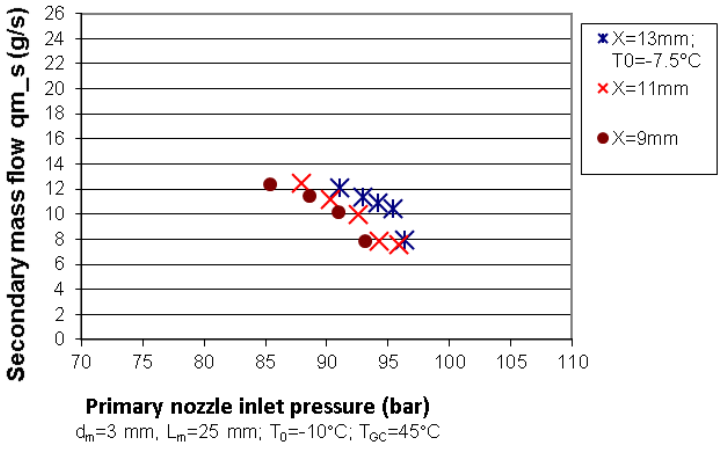

Figure 10: Effect of the distance X on the secondary mass flow for different pressures at the inlet of the primary nozzle with the 3 mm diameter mixing chamber.

The compression ratio, Table 8, increases with increasing pressure at the inlet of the primary nozzle for position $X = 11$ mm and reaches a maximum value of 1.22 for position $X = 13$ mm for a pressure of 91 bar.

Table 8: Effect of the distance between the motive nozzle and mixing chamber (X) on the compression ratio for different pressures at the inlet of the primary nozzle with the 3 mm diameter mixing chamber ($d_m = 3$ mm, $L_m = 25$ mm; $T_0 = -10$°C and -7.5°C for $X = 13$ mm; $T_{GC} = 45$°C).

X (mm)	P (bar)	CR	P (bar)	CR	P (bar)	CR	P (bar)	CR	P (bar)	CR
9	85.418	1.146	88.576	1.145	90.959	1.144	93.099	1.142	–	–
11	87.961	1.179	90.275	1.180	92.583	1.182	94.222	1.185	95.841	1.189
13	91.055	1.217	92.961	1.218	94.168	1.219	95.396	1.218	96.328	1.213

4.3 Case of the primary nozzle PN3

For a variable CO_2 temperature of 30 to 48°C at the outlet of the gas cooler and a variable evaporation temperature of –14 to +2°C, the maximum entrainment ratio can reach 0.387. It is noted from Table 9 that the optimal distance X is between 6 mm and 13 mm. For a primary fluid pressure of 75 bar and when X increases from 11 mm to 13 mm, the entrainment ratio decreases from 0.204 to 0.168. For $X = 11$ mm, the entrainment ratio is the

Table 9: Effect of the distance between the motive nozzle and mixing chamber (X) on the entrainment ratio for different pressures at the inlet of the primary nozzle with the 3 mm diameter mixing chamber ($d_m = 3$ mm, $L_m = 25$ mm).

X (mm)	P (bar)	U	P (bar)	U	P (bar)	U	P (bar)	U	P (bar)	U
6	78.145	0.200	80.297	0.221	84.233	0.163	86.298	0.209	88.245	0.227
6	90.400	0.211	92.337	0.212	94.245	0.235	96.276	0.248	98.277	0.232
6	100.293	0.228	102.268	0.224	104.271	0.227	106.234	0.252	108.626	0.293
9	76.218	0.207	78.229	0.181	80.350	0.239	82.192	0.245	84.233	0.163
9	86.252	0.227	88.212	0.212	90.291	0.216	92.228	0.221	94.265	0.253
9	96.230	0.227	98.160	0.237	100.248	0.230	102.337	0.246	104.106	0.257
9	106.216	0.274	107.347	0.284	–	–	–	–	–	–
11	72.029	0.199	73.996	0.210	75.958	0.224	77.919	0.274	80.035	0.240
11	82.006	0.240	83.968	0.240	86.014	0.235	88.038	0.235	90.041	0.243
11	92.011	0.239	94.030	0.250	95.935	0.250	97.961	0.260	100.074	0.272
11	102.074	0.284	104.013	0.339	105.960	0.352	107.853	0.387	–	–
13	74.630	0.169	78.610	0.218	80.383	0.237	82.117	0.233	84.546	0.209
13	86.662	0.208	88.939	0.224	90.041	0.243	92.579	0.240	94.541	0.220
13	96.438	0.236	98.434	0.227	100.483	0.238	102.602	0.244	104.591	0.267
13	106.496	0.295	108.092	0.322	–	–	–	–	–	–

highest over the entire pressure range at the inlet of the primary nozzle. The difference between the entrainment ratio for position $X = 6$ mm and 9 mm is insignificant. For a primary fluid pressure of 100 bar and when X increases from 9 mm to 11 mm, the entrainment ratio increases from 0.22 to 0.27. The difference between the entrainment ratio increases and when the pressure reaches 107 bar, the entrainment ratio of 0.283 and 0.387 are recorded, respectively, for these last two positions.

From Fig. 11, it is found that the relative position of the primary nozzle does not significantly affect the compression ratio of the ejector. It appears, in the light of experiments, that the best compression ratios are obtained when $X = 11$ mm. For a primary fluid pressure of 76 bar, when X increases from 9 mm to 11 mm, the compression ratio remains invariable. The secondary flow rate relative to this pressure is 7.07 g/s, Fig. 12, and increases to 18.05 g/s. The primary flow is not influenced by the position. The slight difference observed in Fig. 13 is mainly due to different temperatures at the outlet of the gas cooler.

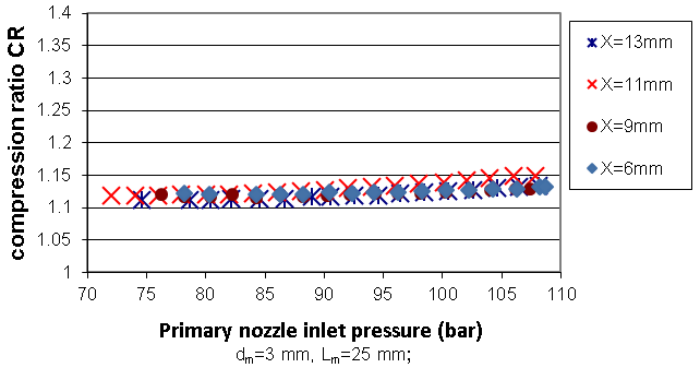

Figure 11: Effect of the distance X on the compression ratio for different pressures at the inlet of the primary nozzle with the 3 mm diameter mixing chamber.

Three primary nozzles were tested and the results of these experiments are presented in Figs. 8 to 16. It is found that:

- the entrainment rate increases when the diameter at the throat of the driving nozzle increases for a given value of X,
- the optimum X value for the nozzles studied is between 11 mm and 13 mm,
- these results are in perfect agreement with the results obtained by Lawrence and Elbel [35] and Liu *et al.* [32, 38, 40].

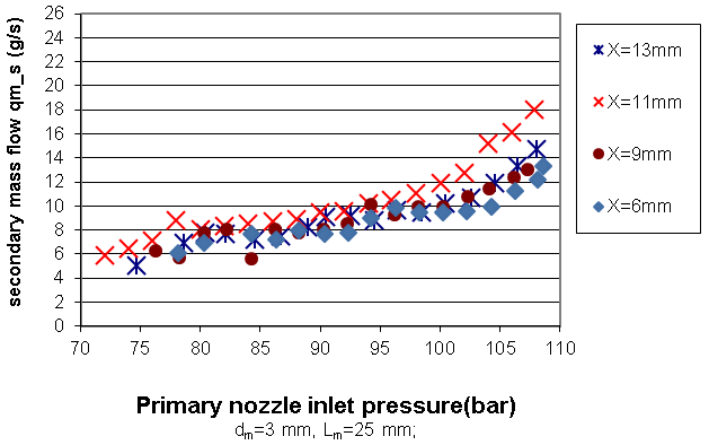

Figure 12: Effect of the distance X on the secondary mass flow rate for different pressures at the inlet of the primary nozzle with the 3 mm diameter mixing chamber.

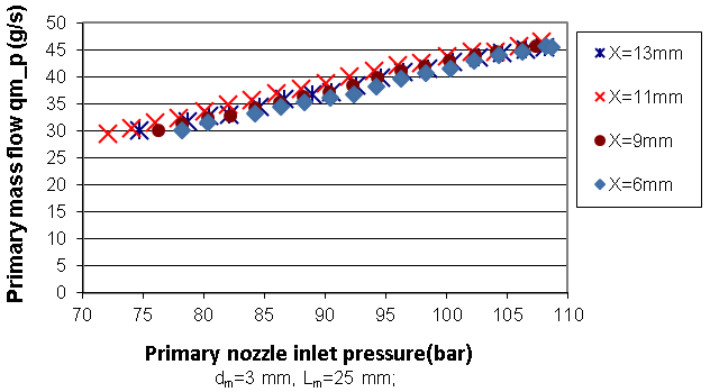

Figure 13: Effect of the distance X on the primary mass flow rate for different pressures at the inlet of the primary nozzle with the 3 mm diameter mixing chamber.

From the analysis carried out for different operating conditions, it is found that an optimum position exists, making it possible to obtain the highest entrainment ratio [38, 40]. This position is 11 mm for primary nozzles with a divergence angle of 2°. Analysis has shown that this position is invariable with the diameter of the mixing chamber. Figure 14 illustrates the effect of the distance between the motive nozzle and mixing chamber (X) on the entrainment ratio (U) for the case of the primary nozzle PN1 using the mixing chamber with a diameter of 5 mm and a constant section length of

25 mm. At a variable CO_2 temperature from 37°C to 65°C at the outlet of the gas cooler and a variable evaporation temperature from −8°C to +2°C, the maximum entrainment ratio of the system can reach 0.308.

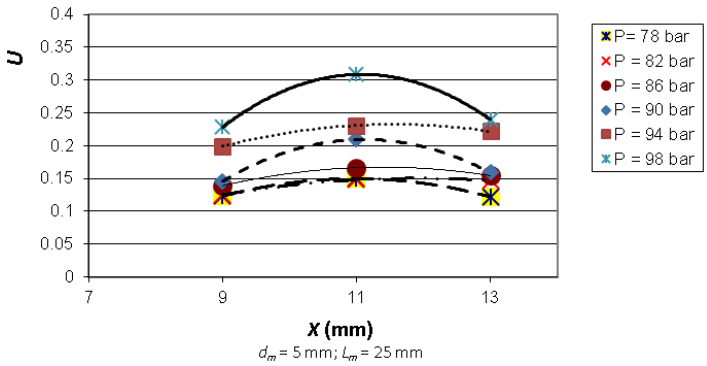

Figure 14: Effect of the distance X on the entrainment ratio for different pressures at the inlet of the primary nozzle with the 5 mm diameter mixing chamber.

The experimental tests also concerned the diameter of the mixing chamber (d_m) and the angle A of the driving nozzles. They revealed that:

- an optimum distance X exists to obtain the highest entrainment ratio. This distance for the primary nozzles having a diverging angle of 2° is 11 mm. The analysis has shown that this position is invariable with the diameter of the mixing chamber, Fig. 14;

- two primary nozzles having a diverging angle of 5° and 7° were tested. It appears from the experiments that the optimum positions are 9 mm and 6 mm, respectively, which differs from the position of the primary nozzles having a diverging angle of 2°, Figs. 15, 16.

The decrease in the entrainment ratio, if the distance X increases when the diverging angle becomes greater, can be explained by the fact that the increase in the outlet section of the primary nozzle opposite to the section of the mixing chamber causes the reduction of the cross-section useful for the flow of the secondary flow.

The entrainment ratio depends significantly on the distance X and there is an optimum distance. This distance essentially depends on the geometry of the primary nozzle, in particular on the angle of divergence and on the pressure at the inlet of the driving nozzle. Three distances have been identified as the optimum distance, namely 6, 9, and 11 mm for three angles

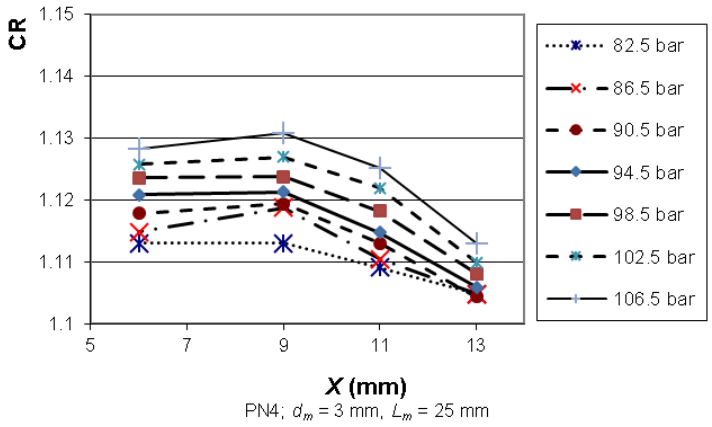

Figure 15: Effect of the distance X on the compression ratio for different pressures at the inlet of the primary nozzle, PN4.

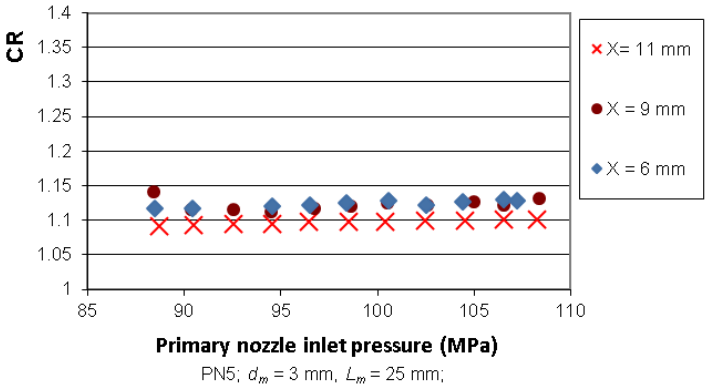

Figure 16: Effect of pressures at the inlet of the primary nozzle for different distances X on the compression ratio, PN5, $d_m = 3$ mm.

of divergence3 of the driving nozzle – 7°, 5°, and 2°, respectively. These distances depend neither on the throat diameter of the primary nozzle nor on the diameter of the mixing chamber, Fig. 16.

Two methods are followed to assess the performance of the ejector:

- in the first method, a constant speed is considered (this method is followed by Liu *et al.* [32]),
- the second method consists in varying the speed and maintaining the evaporating and the outlet gas cooler temperatures constants. This

method makes it possible to better compare the performances of the ejector for defined operating conditions. This method is adopted by Elbel and Hrnjak [1].

It appears from the experiments that:

- the optimum distance X obtained for the 2° diverging angle nozzles is 11 mm for mixing chamber diameters 3, 4 and 5 mm. The experimental study by Liu *et al.* [32] has shown that the entrainment ratio, the compression ratio, the cooling capacity and the COP reach the maximum level when the distance X is 3 times the diameter of the mixing chamber. The diameter of the mixing chamber used in their case is 4 mm. The optimum distance X is 12 mm, a distance almost identical to that found in this study for the three diameters studied. Thus, the factor 3 times the diameter does not seem valid and the position of the primary nozzle is independent of the diameter of the mixing chamber [40];
- for a given geometry and operating conditions of the ejector, two optimum distances between the motive nozzle and mixing chamber (X_{opt}) exist to cover the entire operating pressure range. The use of an ejector with a removable driving nozzle can offer a more flexible operation than a fully fixed geometrical assembly [41].

Table 10 summarizes the values of X_{opt} as a function of d_m, α, L_m, and d^*. It appears from the table that X_{opt} essentially depends on the geometry of the primary nozzle, in particular the diverging angle and the inlet primary nozzle pressure. This pressure is in the range from 80 bar to 100 bar.

Table 10: The optimum dimensionless distances between the motive nozzle and mixing chamber (X^*_{opt}) with the 25 mm length of the mixing chamber ($L_m = 25$ mm) as a function of the throat diameter (d^*) and diverging angle (α) of the primary nozzle.

X^*_{opt} (–)	d^* (mm)	α (°)
11/3	1.0	2
11/4	1.2	2
11/5	1.2	2
11/3	0.9	2
9/3	0.9	5
6/3	0.9	7

As long as the diameter of the cylindrical jet of the primary flow is less than the diameter of the mixing chamber, there will be no blockage of the secondary flow. This explains the results obtained for the same operating conditions and for the same geometric characteristics (d_m, L_m, and d^*) except for the angle α. The larger α, the smaller X_{opt},

5 Conclusion

The steady-state performance of a CO_2 refrigerating system using a two-phase ejector with the variation of ejector geometrical parameters such as the motive nozzle throat diameter, the distance between motive nozzle and diffuser, and the mixing chamber diameter were carried out. The results showed that there exist optimum design parameters in each test.

The performance of the designed ejector was therefore determined during an experimental campaign, which showed that the performance of the CO_2 transcritical system is dependent on the operating conditions and the geometry of the ejector. Thus, the impact of several geometric parameters (the position of the driving nozzle, its diverging angle, its throat diameter, the diameter of the mixing chamber and its length) and thermodynamic parameters on the performance of the ejectors was analysed.

The results relating to the geometric parameters show that:

- The position of the primary nozzle affects significantly the performance of the ejector. It appears that the best performance is obtained when the outlet from the primary nozzle is located at positions defined by:
  - $X^*_{\text{opt}} = 3.66$ for the primary nozzles having an angle of 2°,
  - $X^*_{\text{opt}} = 3$ for the primary nozzles having an angle of 5°,
  - $X^*_{\text{opt}} = 2$ for the primary nozzles having an angle of 7°.

  These positions remain valid for different diameters at the throat of the nozzle, the same diverging angle, different diameters of the mixing chamber and different inlet primary nozzle pressures;
- The throat diameter of the primary nozzle also has a significant influence on performance. The primary flow increases with the throat diameter of the primary nozzle and thus, the PN1 nozzle of diameter 1.2 mm gives a secondary mass flow greater than that of the other nozzles;

- The diameter of the mixing chamber is a crucial parameter in the performance of the ejector. The impact of this factor on the functioning of the ejector has been evaluated experimentally. It has been shown that the best performance is achieved for the mixing chamber with a diameter of 3 mm and having a constant section length of 25 mm.

A diverging angle of the driving nozzle of 2° gives maximum performance in terms of entrainment ratio and compression ratio for operating conditions. The optimization of the system performance (entrainment ratio and compression ratio) can be obtained by adjusting the dimensions of the various components of the ejector.

Honour to Ali BOUZRARA

This article is dedicated to the memory of Ali Bouzrara, Research Professor at the Energetic and Environment Research Laboratory at Tunis El Manar University, who died in 2018.

Acknowledgement This work has been supported by the Centre for Energy and Thermal Sciences of the INSA of Lyon. All the gratitude and the recognition to the Centre for Energy and Thermal Sciences of the INSA of Lyon, who made available all the equipment necessary to carry out this experimental work.

Received 30 September 2020

References

[1] Elbel S., Hrnjak P.: *Experimental validation of a prototype ejector designed to reduce throttling losses encountered in transcritical R744 system operation*. Int. J. Refrig. **31**(2008), 3, 411–422.

[2] Liu J.P., Chen J.P., Chen Z.J.: *Thermodynamic analysis on transcritical R744 vapor compression/ejection hybrid refrigeration cycle*. In: Prelim. Proc. 5th IIR Gustav Lorentzen Conf. on Natural Working Fluids, Guangzhou 2002, 184–188.

[3] Jeong J., Saito K., Kawai S., Yoshikawa C., Hattori K.: *Efficiency enhancement of vapor compression refrigerator using natural working fluids with two-phase flow ejector*. In: Proc. 6th IIR-Gustav Lorentzen Conf. on Natural Working Fluids at Glasgow 2004, CD-ROM.

[4] Jian-qiang Deng, Pei-xue Jiang, Tao Lu, Wei Lu: *Particular characteristics of transcritical CO_2 refrigeration cycle with an ejector*. Appl. Therm. Eng. **27**(2007), 381–388.

[5] Da Qing Li, Groll E.A.: *Transcritical CO_2 refrigeration cycle with ejector-expansion device*. Int. J. Refrig. **28**(2005), 5, 766–773.

[6] Ksayer E.B., Clodic D.: *Enhancement of CO_2 refrigeration cycle using an ejector: 1D analysis*. In: Proc. Int. Refrigeration and Air Conditioning Conf., Purdue 2026, Purdue Univ. R058.2006.

[7] Bartosiewicz Y., Aidoun Z., Mercadier Y.: *Numerical assessment of ejector operation for refrigeration applications based on CFD*. Appl. Therm. Eng. **26**(2006), 5-6, 604–612.

[8] Petrenko V.O., Huang B.J., Ierin V.O.: *Design-theoretical study of cascade CO_2 sub-critical mechanical compression/butane ejector cooling cycle*. Int. J. Refrig. **34**(2011), 7, 1649–1656.

[9] Martel S.: *Étude numérique d'un écoulement diphasique critique dans un convergent-divergent*. PhD thesis, Université de Sherbrooke, Sherbrooke 2013 (in French).

[10] Marynowski T.: *Étude expérimentale et numérique d'écoulements supersoniques en éjecteur avec et sans condensation*. PhD thesis, Université de Sherbrooke, Sherbrooke 2007 (in French).

[11] Scott D., Aidoun Z., Ouzzane M.: *An experimental investigation of an ejector for validating numerical simulations*. Int. J. Refrig. **34**(2011), 7, 1717–1723.

[12] Chen H., Zhu J., Ge J., Lu W., Zheng L.: *A cylindrical mixing chamber ejector analysis model to predict the optimal nozzle exit position*. Energy **208**(2020), 118302.

[13] Mondal S., De D.: *Performance assessment of a low-grade heat driven dual ejector vapor compression refrigeration cycle*. Appl. Therm. Eng. **179**(2020), 115782.

[14] Ringstad K.E., Allouche Y., Gullo P., Banasiak K., Hafner A.: *A detailed review on CO_2 two-phase ejector flow modeling*. Thermal Sci. Eng. Progress **20**(2020), 100647.

[15] Yu B., Yang J., Wang D., Shi J., Chen J.: *An updated review of recent advances on modified technologies in transcritical CO_2 refrigeration cycle*. Energy 189(2019), 116147.

[16] Chen W., Liu M., Chong D., Yan J., Little A.B., Bartosiewicz Y.A.: *1D model to predict ejector performance at critical and sub-critical operational regimes*. Int. J. Refrig. **36**(2013), 6, 1750–1761.

[17] Banasiak K., Hafner A., Andresen T.: *Experimental and numerical investigation of the influence of the two-phase ejector geometry on the performance of the R744 heat pump*. Int. J. Refrig. **35**(2012), 6, 1617–1625.

[18] Domanski P.A.: *Theoretical Evaluation of the Vapor Compression Cycle With a Liquid-Line/Suction-Line Heat Exchanger, Economizer, and Ejector*. National Institute of Standards and Technology, NISTIR-5606, 1995.

[19] Elbel S.W., Hrnjak P.S.: *Effect of internal heat exchanger on performance of transcritical CO_2 systems with ejector*. In: Proc. 10th Int. Refrigeration and Air Conditioning Conf. Purdue 2004, R166, West Lafayette 2004.

[20] Kornhauser A.A.: *The use of an ejector as a refrigerant expander*. In: Proc. USNC/IIR-Purdue Refrigeration Conf., Purdue Univ.,West Lafayette 1990, 10–19.

[21] Lawrence N., Elbel S.: *Experimental and analytical investigation of automotive ejector air-conditioning cycles using low-pressure refrigerants*. In: Proc. Int. Refrigeration and Air Conditioning Conf., Purdue, July 16-19, 2012, 1169, 1–10.

[22] Liu F., Li Y., Groll E.A.: *Performance enhancement of CO_2 air conditioner with a controllable ejector*. Int. J. Refrig. **35**(2012), 6, 1604–1616.

[23] Domanski P.A.: *Minimizing throttling losses in the refrigeration cycle*. In: Proc. 19th Int. Congress of Refrigeration, Hague 1995, 766–773.

[24] Varga S., Oliveira A., Diaconu B.: *Influence of geometrical factors on steam ejector performance – A numerical assessment*. Int. J. Refrig. **32**(2009), 7, 1694–1701.

[25] Sarkar J.: *Optimization of ejector-expansion transcritical CO_2 heat pump cycle*. Energy **33**(2008), 9, 1399–1406.

[26] Elbel S.: *Historical and present developments of ejector refrigeration systems with emphasis on transcritical carbon dioxide air-conditioning applications*. Int. J. Refrig. **34**(2011), 7, 1545–1561.

[27] Lee J.S., Kim M.S., Kim M.S.: *Experimental study on the improvement of CO_2 air conditioning system performance using an ejector*. Int. J. Refrig. **34**(2011), 7, 1614–1625.

[28] Lucas C., Koehler J.: *Experimental investigation of the COP improvement of a refrigeration cycle by use of an ejector*. Int. J. Refrig. **35**(2012), 6, 1595–1603.

[29] Nakagawa M., Marasigan A.R., Matsukawa T., Kurashina A.: *Experimental investigation on the effect of mixing length on the performance of two-phase ejector for CO_2 refrigerationcycle with and without heat exchanger*. Int. J. Refrig. **34**(2011), 7, 1604–1613.

[30] Nakagawa M., Marasigan A.R., Matsukawa T.: *Experimental analysis on the effect of internal heat exchanger in transcritical CO_2 refrigeration cycle with two-phase ejector*. Int. J. Refrig. **34**(2011), 7, 1577–1586.

[31] Nakagawa M., Marasigan A.R., Matsukawa T.: *Experimental analysis of two phase ejector system with varying mixing cross-sectional area using natural refrigerant CO_2*. Int. J. Air-Cond. Refrig. **18**(2010), 4, 297–307.

[32] Liu F., Groll E.A., Li D.: *Investigation on performance of variable geometry ejectors for CO_2 refrigeration cycles*. Energy **45**(2012), 1, 829–839.

[33] Liu F., Groll E.A.: *Analysis of a two-phase flow ejector for transcritical CO_2 cycle*. Int. Refrig. Air Cond. Conf., Purdue, July 14–17, 2008, 924.

[34] Liu F., Groll E.A.: *Study of ejector efficiencies in refrigeration cycles*. Appl. Therm. Eng. **52**(2013), 2, 360–370.

[35] Lawrence N., Elbel S.: *Experimental investigation on the effect of evaporator design and application of work recovery on the performance of two-phase ejector liquid recirculation cycles with R410A*. Appl. Therm. Eng. **100**(2016), 398–411.

[36] Van Nguyen V., Varga S., Soares J., Dvorak V., Oliveira A.C.: *Applying a variable geometry ejector in a solar ejector refrigeration system*. Int. J. Refrig. **113**(2020), 187–195.

[37] Pereira P.R., Varga S., Soares J., Oliveira A.C., Lopes A.M., de Almeida F.G., Carneiro J.F.: *Experimental results with a variable geometry ejector using R600a as working fluid.* Int. J. Refrig. 46(2014), 77–85.

[38] Liu F., Groll E.: *A preliminary study of the performance enhancement of a dual-mode heat pump using an ejector.* In: Proc. 25th IIR Int. Cong. of Refrigeration, ICR2015, Yokohama, Aug. 16-22, 2015, 16–22.

[39] Eames I.W., Wu S., Worall M., Aphornratana S.: *An experimental investigation of steam ejectors for application in jet-pump refrigerators powered by low-grade heat.* P. I. Mech. Eng. A-J Pow. **A 213**(1999), 5, 351–361.

[40] Lee J.S., Kim M. Se, Kim M. Soo: *Experimental study on the improvement of CO_2 air conditioning system performance using an ejector.* Int. J. Refrig. **34**(2011), 7, 1614–1625.

[41] Bouzrara A.: *Etude expérimentale des éjecteurs- application à la récupération de l'énergie de détente des machines frigorifiques au CO_2.* PhD thesis, INSA Lyon (CETHIL)-ENI Tunis 2018 (in French).